radiotherapy and chemotherapy is usually employed either for symptomatic or resectability improvement.[29] Despite the use of multimodality therapy, 5-year survival rates of patients with LRRC remain 22–31% and local control rates 50–71%.[30–33] On the other hand, CIRT alone has an overall survival rate of 42.8% and local control rate of 81% at 5 years.[7] By analyzing these 5-year survival rates and local control rates based on our calculated mean cost of ¥4 803 946 for CIRT and ¥4 611 110 for multimodality treatment, CIRT seems a cost-effective treatment modality for LRRC (Table 4). In addition, the wide range of cost and high cost at GUH (Table 2) was mainly a consequence of differences in survival (Fig. 1) and variation in days of admission (Table 2) that could be linked to severity of treatment complications (Table 5). For example, the absolute total costs for patients #1 and #2 in the multimodality treatment group were higher than the other patients in the same group (about ¥8 million) due to their long days of admission (Table 2) including admission to the intensive care unit. The same applies to patient #8 in the CIRT group (Table 2). On the other hand, patients #9 and #10 in the multimodality treatment group had a cost of about ¥1.8 million (Table 2) because they had the least survival among the group and died within the first year (Fig. 1).

The present study included all direct costs for 2 years of follow-up from the time of recurrence. Although CIRT yielded better outcomes, there was insignificant difference between the mean costs of both treatment modalities. The calculated ICER in terms of gain in overall survival probability due to carbon ion radiotherapy is ¥6428 per 1% increase in survival.

The limitations of this study are that it is retrospective and that it could not include all indirect costs, such as loss of economic productivity during and after the treatment as well as the cost of intangibles. However, the duration of radiation therapy and length of hospital stay related to the complications and toxicity, are both in favor of CIRT and may provide some clues regarding indirect costs. Additionally, in the current 2-year follow up study, the local control rate could not be evaluated due to improper documentation of exact date of distant metastasis at GUH. However, due to the latter limitation and a probability of falling survival rates beyond the 2 years, we additionally analyzed data in the literature representing both treatment modalities, but with longer follow-up (5-year survival and control rates) and larger sample sizes (Table 4).

In conclusion, our analysis provides some evidence that CIRT could be cost-effective in the treatment of LRRC. To the best of our knowledge, this is the first cost-effectiveness study of carbon ion beam radiotherapy including all direct costs. However, it is also necessary to take into account the indirect costs, which means that future prospective studies are needed. Yet, to perform a prospective cost-effectiveness study before implementing a new technology still raises ethical concerns.[34–36] In general, there is a lack of information concerning the cost-effectiveness of other cancers that are effectively treated by CIRT such as bone and soft tissue, lung, liver, prostate, and head and neck cancers.[7] Additionally, there is little data available about the relative cost-effectiveness of CIRT compared with proton radiotherapy. These may represent important areas for future research.

Acknowledgments

The authors gratefully thank Y. Suzuki, W. Aljahdari, T. Asao, H. Kuwano, T. Kamada, and H. Tsujii for their feedback.

Abbreviations

RT	radiotherapy
UICC/6th	International Union Against Cancer tumor-node-metastasis (TNM) classification, sixth edition
DPC	diagnosis procedure combinations
RT	radiotherapy
ICER	incremental cost-effective ratio
NCI-CTC	National Cancer Institute – Common Toxicity Criteria, version 2
RTOG/EORTC	Radiation Therapy Oncology Group/European Organization for Research and Treatment of Cancer

References

1 Parkin D, Bray F, Ferlay J *et al.* Global cancer statistics 2002. *CA Cancer J Clin* 2005; **55**: 74–108.
2 Ferlay J, Bray F, Pisani P *et al. Globocan 2002. Cancer Incidence, Mortality and Prevalence Worldwide. IARC Cancer Base No. 5 Version 2.0.* Lyon, France: IARC Press, 2004.
3 Ohno Y, Nakamura T, Murata K *et al.* Prediction of cancer incidence in Japan. In: Oshima A, Kuroiwa T, Tajima K, eds. *Cancer Statistic -2004.* Tokyo: Shinohara Shuppan, 2004; 201–17.
4 Kobayashi A, Sugito M, Ito M *et al.* Predictors of successful salvage surgery for local pelvic recurrence of rectosigmoid colon and rectal cancers. *Surg Today* 2007; **37**: 853–9.
5 Bosanquet N, Sikora K. The economics of cancer care in the UK. *Lancet Oncol* 2004; **5**: 568–74.
6 Ministry of Health, Labour and Welfare. National medical care expenditure trends in Japan (1977–2002). [Cited 12 March 2009.] Available from URL: http://ganjoho.ncc.go.jp/public/statistics/backnumber/odjrh3000000h332-att/data16.pdf.
7 Tsujii H, Kamada T, Baba M *et al.* Clinical advantages of carbon-ion radiotherapy. *New J Phys* 2008; **10**: 075009.
8 Herndon J, Hwang R, Bozic K. Healthcare technology and technology assessment. *Eur Spine J* 2007; **16**: 1293–302.
9 Jakel O, Land B, Combs S *et al.* On the cost-effectiveness of Carbon ion radiation therapy for skull base chordorna. *Radiother Oncol* 2007; **83**: 133–8.
10 Okamura S, Kobayashi R, Sakamaki T. Case-mix payment in Japanese medical care. *Health Policy* 2005; **74**: 282–6.
11 Yasunaga H, Ide H, Imamura T *et al.* Impact of the Japanese diagnosis procedure combination-based payment system on cardiovascular medicine-related costs. *Int Heart J* 2005; **46**: 855–66.
12 Asao T, Sakurai H, Harashima K *et al.* The synchronization of chemotherapy to circadian rhythms and irradiation in pre-operative chemoradiation therapy with hyperthermia for local advanced rectal cancer. *Int J Hyperthermia* 2006; **22**: 399–406.
13 Wildner M. Health economic issues of screening programmes. *Eur J Pediatr* 2003; **162**: S5–7.
14 Tsujii H, Mizoe J, Kamada T *et al.* Clinical results of carbon ion radiotherapy at NIRS. *J Radiat Res* 2007; **48**: A1–13.
15 Shibuya H, Tsujii H. The structural characteristics of radiation oncology in Japan in 2003. *Int J Radiat Oncol Biol Phys* 2005; **62**: 1472–6.
16 Tsujii H, Kamada T, Debus J. Overview of experience with heavier charged particle radiotherapy. In: Delaney TF, Kooy HM, eds. *Proton and Charged Particle Radiotherapy.* Philadelphia, PA: Lippincott Williams and Wilkins, 2008; 123.
17 Nakagawa Y, Yoshihara H, Kageji T *et al.* Cost analysis of radiotherapy, carbon ion therapy, proton therapy and BNCT in Japan. *Appl Radiat Isot* 2009; **67**: S80–3.
18 Muramatsu M, Kitagawa A, Drentje AG *et al.* The compact electron cyclotron resonance ion source KeiGM for the carbon ion therapy facility at Gunma University. *Rev Sci Instrum* 2010; **81**: 02A327–3.
19 48th meeting of Particle Therapy Co-Operative Group (PTCOG). Meeting abstract "Current Status of Gunma University Heavy Ion Medical Center". [Cited 21 March 2010.] Available from URL: http://www.egms.de/static/en/meetings/ptcog2009/09ptcog146.shtml.
20 Brower V. Carbon ion therapy to debut in Europe. *J Natl Cancer Inst* 2009; **101**(2): 74–6.
21 Ando K, Kase Y. Biological characteristics of carbon-ion therapy. *Int J Radiat Biol*2009; **85**(9): 715–28.
22 Morrison A. Carbon Ion Radiation Therapy [Environmental Scan issue 3]. Ottawa: Canadian Agency for Drugs and Technologies in Health (cadth);

doi: 10.1111/j.1349-7006.2010.01604.x
© 2010 Japanese Cancer Association

2009. [Cited 22 March 2010.] Available from URL: http://www.cadth.ca/media/pdf/hta_Carbon-Ion-Radiation-Therapy_es-issue-3_e.pdf.
23 Jones B. Joint symposium 2009 on carbon ion radiotherapy. *Br J Radiol* 2009; **82**: 884–9.
24 Goitein M, Jermann M. The relative costs of proton and X-ray radiation therapy. *Clin Oncol (R Coll Radiol)* 2003; **15**: S37–50.
25 Pommier P, Gueye N, Buron C *et al.* Medico-economic and Spatial Modelization for decision making in innovative therapies: application to light ions therapy projects in Europe. *Radiother Oncol* 2006; **81**: S411.
26 Schulz-Ertner D, Haberer T, Scholz M *et al.* Acute radiation-induced toxicity of heavy ion radiotherapy delivered with intensity modulated pencil beam scanning in patients with base of skull tumors. *Radiother Oncol* 2002; **64**: 189–95.
27 Tveit K, Wiig J, Olsen D *et al.* Combined modality treatment including intraoperative radiotherapy in locally advanced and recurrent rectal cancer. *Radiother Oncol* 1997; **44**: 277–82.
28 Knol H, Hanssens P, Rutten H *et al.* Effect of radiation therapy alone or in combination with surgery and/or chemotherapy on tumor and symptom control of recurrent rectal cancer. *Strahlenther Onkol* 1997; **173**: 43–9.
29 Valentini V, Morganti A, Gambacorta M *et al.* Preoperative hyperfractionated chemoradiation for locally recurrent rectal cancer in patients previously irradiated to the pelvis: a multicentric phase II study. *Int J Radiat Oncol Biol Phys* 2006; **64**: 1129–39.
30 Willett C, Shellito P, Tepper J *et al.* Intraoperative electron beam radiation therapy for recurrent locally advanced rectal or rectosigmoid carcinoma. *Cancer* 1991; **67**: 1504–08.
31 Bussieres E, Gilly F, Rouanet P *et al.* Recurrences of rectal cancers: results of a multimodal approach with intraoperative radiation therapy. French group of intraoperative radiation therapy. *Int J Radiat Oncol Biol Phys* 1996; **34**: 49–56.
32 Valentini V, Morganti A, De Franco A *et al.* Chemoradiation with or without intraoperative radiation therapy in patients with locally recurrent rectal carcinoma. *Cancer* 1999; **86**: 2612–24.
33 Wiig J, Poulsen J, Larsen S, Braendengen M, Waehre H, Gierckskiy K. Total pelvic exenteration with preoperative irradiation for advanced primary and recurrent rectal cancer. *Eur J Surg* 2002; **168**: 42–8.
34 Bentzen SM. Randomized controlled trials in health technology assessment: overkill or overdue? *Radiother Oncol* 2008; **86**: 142–7.
35 Goitein M, Cox JD. Should randomized clinical trials be required for proton radiotherapy? *J Clin Oncol* 2008; **26**: 175–6.
36 Suit H, Kooy H, Trofimov A *et al.* Should positive phase III clinical trial data be required before proton beam therapy is more widely adopted? No. *Radiother Oncol* 2008; **86**: 148–53.

© 2010 Japanese Cancer Association

Journal of Surgical Oncology 2010;101:97–99

HOW I DO IT

Particle Beam Radiotherapy With a Surgical Spacer Placement for Advanced Abdominal Leiomyosarcoma Results in a Significant Clinical Benefit

TAKUMI FUKUMOTO, MD, PhD,[1] SHOHEI KOMATSU, MD,[1] YUICHI HORI, MD, PhD,[1]*
MASAO MURAKAMI, MD, PhD,[2] YOSHIO HISHIKAWA, MD, PhD,[2] AND YONSON KU, MD, PhD[1]
[1]Division of Hepato-Biliary-Pancreatic Surgery, Department of Surgery, Kobe University Graduate School of Medicine, Kobe, Japan
[2]Department of Radiology, Hyogo Ion Beam Medical Center, Tatsuno, Japan

INTRODUCTION

Leiomysarcoma is a rare malignant tumor originating from smooth muscle cells. Because of the limited number of cases, the natural history and optimal treatment have not been clarified. In particular, prognosis of leiomyosarcoma originating from large vessels including the inferior vena cava (IVC) and aorta is extremely poor. Recent data support an aggressive surgical resection combined with adjuvant chemotherapy as the best treatment option for a leiomyosarcoma from the IVC [1,2]. However, the long-term outcome of curative resections for leiomyosarcoma from large vessels has been disappointing. The 5-year survival rates obtained with absolute curative resections were observed to range from 34.8% to 53.3% [1,2]. Hines et al. [2] suggested that radiation therapy after a surgical resection may prolong survival. It should be noted, however, that an absolute curative resection was performed in all of their cases and the effectiveness of chemotherapy and radiotherapy were assessed in the framework of adjuvant therapy. There is no report about the treatment of an unresectable leiomyosarcoma and the overall survival rate.

Particle beam radiotherapy is a new mode of radiotherapy that has an inherent advantage over photon radiotherapy. Particle beams, such as proton and carbon ion beams, show an increase in energy deposition with penetration depth up to a sharp maximum at the end of their range to form the so-called Bragg peak. It thus permits delivery of higher doses of radiation to the tumor, which may lead to profoundly improved tumor eradication. Recent results from major centers have shown the therapeutic superiority of particle radiotherapy for various kinds of malignant tumors [3,4]. However, the application of particle beam radiotherapy for abdominal malignant tumors is restricted because most of them come in contact with the intestine that cannot tolerate the radical dose of particle beams. Several studies have investigated the risk factors related to late gastrointestinal tract disturbance after radiotherapy. Ishikawa et al. [5] assessed that the dosimetric parameter was a very important factor in the occurrence of gastrointestinal bleeding after particle radiotherapy. Gastrointestinal disturbances, such as ulcer formation and colitis, generally occur within several months after the completion of particle radiotherapy. However, the irradiated volume of a marginal tumor is normally limited to make it lower than the maximum dose in order to prevent any toxicity to the nearby gastrointestinal tract. To overcome this limitation, we developed a novel two-step treatment with a surgical spacer placement and subsequent proton beam radiotherapy and achieved a significant clinical benefit for three patients.

© 2009 Wiley-Liss, Inc.

METHODS

The treatment strategy is an attempt to keep the intestine away from the irradiation field by spacer placement and to perform proton beam radiotherapy with a curative intent. Eight Gore-Tex sheets ($20\,cm \times 15\,cm \times 2\,mm^3$) were superimposed and applied as a spacer to keep safety margin away from the intestine. The spacer was fixed with the retroperitoneum and peritoneum. During the spacer placement surgery, no part of the tumor was resected because it was just a first step to allow proton beam radiotherapy.

PATIENT AND RESULTS

We would show the representative case. A 65-year-old female was diagnosed to have a far advanced leiomyosarcoma measuring $12 \times 12\,cm^2$ that originated from IVC above the level of the aortic bifurcation because of extensive invasion to the unresectable nearby tissues including the spinal cord, the right iliopsoas muscle, right internal and external iliac arteries, and the right urinary tract. The tumor did not fulfill the indication for a curative resection due to the poor prognosis of a far advanced leiomyosarcoma. She was then referred to our department to undergo particle beam radiotherapy. Abdominal MRI after the operation showed the spacer maintained a sufficient open space between the tumor and intestine (Fig. 1A–D, asterisk: the huge tumor, arrowhead: Gore-Tex spacer sheets around the tumor) (Fig. 1D, operative finding of the spacer placement). One month later, she underwent proton beam radiotherapy with 70.4 GyE in 16 fractions over 24 days at Hyogo Ion Beam Medical Center (HIBMC). The dose–distribution curve and dose–volume histogram in treatment planning are shown in Figure 2. Due to the spacer, the digestive tract is located entirely outside the irradiated volume (Fig. 2A). Dose–volume histogram of the clinical target

Takumi Fukumoto and Shohei Komatsu contributed equally to this work.

*Correspondence to: Dr. Yuichi Hori, MD, PhD, Division of Hepato-Biliary-Pancreatic Surgery, Department of Surgery, Kobe University Graduate School of Medicine, 7-5-1 Kusunoki-cho, Chuo-ku, Kobe 650-0017, Japan. Fax: +81-78-382-6307. E-mail: horiy@med.kobe-u.ac.jp

Received 1 July 2009; Accepted 27 August 2009
DOI 10.1002/jso.21417
Published online 1 October 2009 in Wiley InterScience (www.interscience.wiley.com).

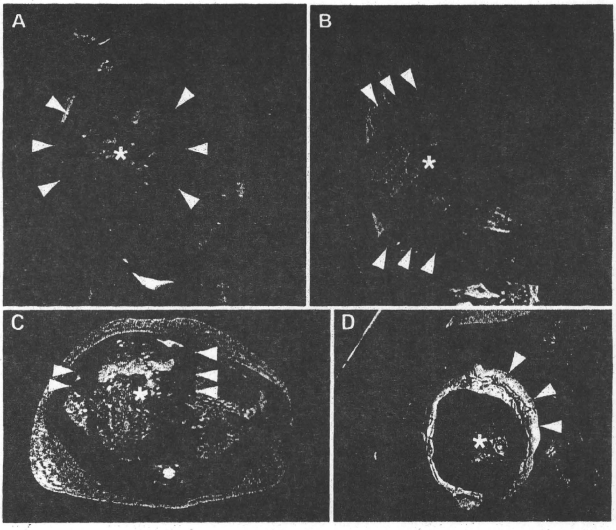

Fig. 1. A–C: Abdominal MRI after the operation for spacer placement. D: The spacer around the tumor using Gore-Tex sheets. The arrowhead shows the spacer around the tumor, and it maintained a sufficient open space between the tumor and the intestine. The asterisk shows the tumor.

volume (CTV) and the intestine are shown. CTV is entirely irradiated with ≥90% of the prescribed dose, and the intestine is hardly irradiated (Fig. 2B). Thus, the spacer placement protected the intestine. Acute and late toxicities associated with treatment were evaluated using both the Radiation Therapy Oncology Group (RTOG) acute radiation morbidity score and RTOG/European Organization for Research and Treatment of Cancer late radiation morbidity score [6]. Acute or late treatment-related toxicities were judged as grade 2. An abdominal MRI taken

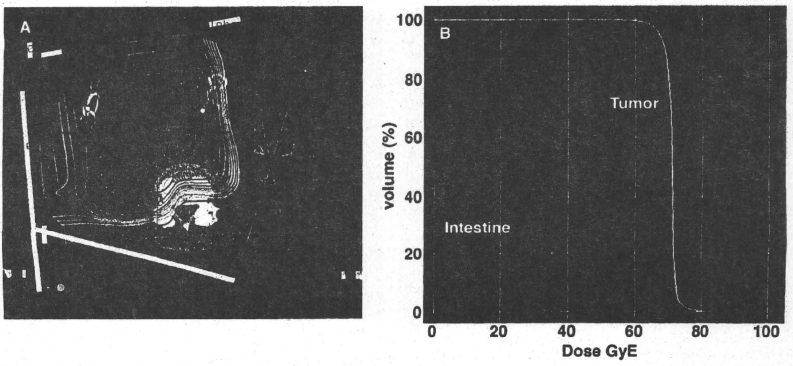

Fig. 2. A: Treatment strategy for proton beam radiotherapy with a total dose of 70.4 GyE in 16 fractions. Isodose curves demonstrate 100% of the prescribed dose at the center and decreasing by 10% of the dose from the inside out. Due to the spacer, the digestive tract is located entirely outside the irradiated volume. B: Dose–volume histogram of the clinical target volume (CTV) and the intestine. CTV is entirely irradiated with ≥90% of the prescribed dose, and the intestine is hardly irradiated.

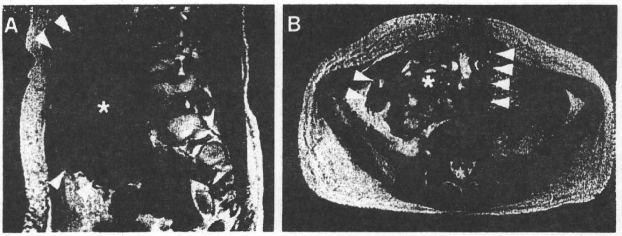

Fig. 3. A,B: Abdominal MRI 6 months after the two-step treatment. The arrowhead shows the spacer. The asterisk shows the distinct shrinkage of the tumor.

TABLE I. Three Cases of Abdominal Leiomyosarcoma Treated With Two-Step Treatment

Age, sex	Tumor origin	Tumor size (cm^2)	Protocol (GyE/Fr)	Disease-free survival (days)
62, Male	Abdominal aorta	13×13	Proton 80.0/32	406
65, Female	Inferior vena cava	12×12	Proton 70.4/16	276
59, Male	Thoraco-abdominal aorta	10×7	Carbon 70.4/16	700

6 months after the two-step treatment showed the distinct shrinkage of the tumor measuring $6 \times 6\,cm^2$ (Fig. 3A,B) and the positron emission tomography scan did not show metastasis to the remote organs throughout the body (data not shown). Since local control is generally defined as no sign of re-growth or new tumors in the treatment volume, this patient was determined to have achieved excellent local control of a far advanced leiomyosarcoma with minimal toxicity. We never remove spacers after particle beam radiotherapy because of the potential surgical risk. We are therefore now developing new spacers made of absorbable mesh.

DISCUSSION

Three cases of unresectable abdominal leiomyosarcomas originating from the abdominal aorta or the IVC were treated with this two-step treatment and all of those cases achieved local control of the primary tumors. From the viewpoint of the disease-free survival, considerable progress was achieved in all three patients (Table I). All three patients showed grade 1 dermatitis as an acute toxicity. While two of three patients reported grade 2 dermatitis as a late toxicity. HBMC is the only facility of particle radiotherapy which both proton and carbon ion beams are available all over the world and we have treated patients using either proton or carbon ion beams since 2001. The policy of choosing beam type at HBMC was as follows: carbon ions show a more favorable dose distribution than protons, however, carbon ions can only be delivered from fixed ports, while a 360° rotating gantry can be used for protons. Treatment plans for both carbon ion and proton were made basically, and better one was chosen for the patient treatment. This type of approach using surgical displacers plus photon (also called X-ray) beam radiotherapy has been previously employed in other malignancies such as rectal cancer [7,8]. However, several lines of evidence support our novel strategy. Particle beams permit favorable dose distributions with a steep dose fall-off at the field borders, suggesting more precise dose localization can be achieved compared with photon beams [4]. Moreover, the use of photon beam is usually restricted to pelvic tumors due to the deposit in surrounding tissues. In contrast, almost no dose of particle beam is deposited in the normal tissue beyond the Bragg peak. We believe surgical spacer placement can keep safety margin from the intestine and full-dose particle beam radiotherapy can be achieved without serious toxicities only by this first step. Furthermore, previous approach with displacer was utilized for postsurgical adjuvant radiotherapy in principle. The rate of local tumor control and acute or late treatment-related toxicities using surgical displacers plus photon were not presented. Although we need further case-control study, our results strongly indicate that this new strategy might potentially be an effective and innovative therapy for unresectable abdominal malignant tumors.

REFERENCES

1. Kieffer E, Alaoui M, Piette JC, et al.: Leiomyosarcoma of the inferior vena cava: Experience in 22 cases. Ann Surg 2006;244: 289–295.
2. Hines OJ, Nelson S, Quinones-Baldrich WJ, et al.: Leiomyosarcoma of the inferior vena cava: Prognosis and comparison with leiomyosarcoma of other anatomic sites. Cancer 1999;85:1077–1083.
3. Brada M, Pijls-Johannesma M, De Ruysscher D: Proton therapy in clinical practice: Current clinical evidence. J Clin Oncol 2007;25: 965–970.
4. Schulz-Ertner D, Tsujii H: Particle radiation therapy using proton and heavier ion beams. J Clin Oncol 2007;25:953–964.
5. Ishikawa H, Tsuji H, Kamada T, et al.: Risk factors of late rectal bleeding after carbon ion therapy for prostate cancer. Int J Radiat Oncol Biol Phys 2006;66:1084–1091.
6. Cox JD, Stetz J, Pajak TF: Toxicity criteria of the Radiation Therapy Oncology Group (RTOG) and the European Organization for Research and Treatment of Cancer (EORTC). Int J Radiat Oncol Biol Phys 1995;31:1341–1346.
7. Sezeur A, Martella L, Abbou C, et al.: Small intestine protection from radiation by means of a removable adapted prosthesis. Am J Surg 1999;178:22–25. discussion 25-26.
8. Waddell BE, Lee RJ, Rodriguez-Bigas MA, et al.: Absorbable mesh sling prevents radiation-induced bowel injury during "sandwich" chemoradiation for rectal cancer. Arch Surg 2000; 135:1212–1217.

Radiol Phys Technol (2010) 3:16–22
DOI 10.1007/s12194-009-0071-4

A parameter study of pencil beam proton dose distributions for the treatment of ocular melanoma utilizing spot scanning

Kenneth Sutherland · Satoshi Miyajima · Hiroyuki Date · Hiroki Shirato · Masayori Ishikawa · Masao Murakami · Mitsuru Yamagiwa · Paul Bolton · Toshiki Tajima

Received: 7 April 2009 / Revised: 4 August 2009 / Accepted: 4 August 2009 / Published online: 19 September 2009
© Japanese Society of Radiological Technology and Japan Society of Medical Physics 2009

Abstract The results of Monte Carlo calculated dose distributions of proton treatment of ocular melanoma are presented. An efficient spot scanning method utilizing active energy modulation, which also minimizes the number of target spots was developed. We simulated various parameter values for the particle energy spread and the pencil beam diameter in order to determine values suitable for medical treatment. We found that a 2.5-mm-diameter proton beam with a 5% Gaussian energy spread was suitable for treatment of ocular melanoma while preserving vision for the typical case that we simulated. The energy spectra and the required proton current were also calculated and are reported. The results are intended to serve as a guideline for a new class of low-cost, compact accelerators.

K. Sutherland (✉) · H. Date · H. Shirato · M. Ishikawa
Hokkaido University School of Medicine
Kita-ku Kita 12 Jo Nishi 5 Chome,
Sapporo 060-0812, Japan
e-mail: kensuth@med.hokudai.ac.jp

K. Sutherland · S. Miyajima
Japan Science and Technology,
Motomachi 4 Chome 1 Ban 8 Go,
Kawaguchi, Saitama 332-0012, Japan

M. Yamagiwa · P. Bolton · T. Tajima
Photo-Medical Research Center, Japan Atomic Energy Agency,
Kizugawa, Kyoto 619-0215, Japan

M. Murakami
Hyogo Ion Beam Medical Center,
Shinguu Chou Hikarimiya 1-2-1,
Tatsuno, Hyogo, Japan

Keywords Proton therapy · Ocular melanoma · Monte Carlo simulation · Laser acceleration

1 Introduction

Proton beams have the potential to decrease normal tissue damage and allow dose escalation in cancer therapy, because the beam profile allows a more localized dose distribution at the tumor than do traditional X-rays. For covering the volume of a target lesion in particle therapy for cancer, two methods have been employed: passive scattering and spot scanning. In the passive scattering method, secondary neutrons from scatter foils, compensators and collimators are a possible source of secondary malignancy [1]. Spot scanning was first proposed as an alternative to passive scattering methods by Kanai et al. [2] and was further investigated by Lomax et al. [3]. Spot scanning utilizes magnetic and mechanical scanning of a pencil proton beam such that individually weighted Bragg peaks are distributed under computer control [4]. For spot scanning, there is no need for patient-specific collimators, thereby reducing the whole-body neutron dose to the patient. Another advantage is that most of the particles from the accelerator can be delivered to the patient, rather than being absorbed by collimators or compensators, and therefore this method is potentially more efficient.

In this work, we present the results of Monte Carlo simulations of proton dose distributions in which we used parameterized proton beams applied to ocular melanoma. We hope that the results of this study will serve as a guide for researchers developing proton facilities for medical treatment. We comment on the potential relevance of laser-accelerated protons [5–8] for the treatment of ocular melanoma, which requires lower proton energies than do more

deeply seated tumors, as well as relatively lower doses (fewer protons) because such tumors are typically small. However, the results should be applicable to proton therapy in general.

2 Materials and methods

2.1 Monte Carlo simulation speed improvements

Geant4 [9] version 8.0p1 was used for these simulations. Geant4 has been validated previously for medical-physics applications [10]. In order to improve the execution speed, we modified the particle navigation library following Jiang and Paganetti [11]. To improve efficiency on a PC cluster, we also developed a custom parallelization of Geant4 [12]. Simulations yield exactly the same results when running in parallel on a cluster or on a single processor as long as random-number-generator seed values are maintained and are set at the beginning of each event.

Following Jiang and Paganetti [11], four physics processes were registered in the Geant4 physics list for proton interactions: proton elastic scattering (*G4HadronElasticProcess*), proton inelastic scattering (*G4HadronInelasticProcess*), ionization (*G4hLowEnergyIonisation*) and multiple scattering (*G4MultipleScattering*). For improved efficiency, only secondary protons and neutrons were tracked. The energy from secondary electrons was deposited locally because the range was assumed to be less than 1 mm in water. The Geant4 maximum step size was limited to 1 mm.

2.2 Radiation treatment simulation software

We developed an application, which investigates the effects of the proton beam diameter and energy spread on the dose distribution. The software allows the user to open a series of DICOM CT images, and specify the target volume, one or more gantry positions and various beam characteristics. The user can also enter the particle (i.e., event) count. We chose a particle count of 1 million for this study, which we determined to be sufficient for good energy deposit distribution statistics with a reasonable processing time.

We used a series of 11 CT images of a disease-free human head with a slice thickness of 2.5 mm and a pixel spacing of 0.3125 mm. The CT pixel value (in Hounsfield units) of each voxel was used for determining the voxel material. Each material was assigned a density and a chemical composition according to the data provided by Schneider et al. [13]. The software generates files, which specify the different voxel materials and an event list containing the initial source position, direction and energy of each particle in the simulation. The dose accumulation grid had the same size and dimensions as the CT data: $512 \times 512 \times 11$; i.e., we did not subsample or smoothen the CT values.

A database of depth and lateral dose profile curves was pre-computed with the use of the Monte Carlo package *Particle and Heavy Ion Transport Code System* (PHITS) [14, 15]. This database was used by our planning software for determining the initial energy peak, energy spread and spot spacing. Depth–dose curves were computed for proton beams incident on water with energies from 30 to 250 MeV in 1-MeV increments. Four values of the Gaussian energy spread were computed: 0, 5, 10 and 15%, at a depth resolution of 0.1 mm. Lateral offset tables were computed for energies from 30 to 200 MeV in 1-MeV increments, with the use of the same energy spread values, 0, 5, 10, and 15%, and with beam diameters of 0, 1.25, 2.5, 5 and 10 mm. The tables were stored in a binary format, which minimized the time necessary for reading of the data by the planning software.

An initial weighting factor was assigned to each target spot, which was used for determining the particle count. The deepest spot (associated with the highest energy) along a beam is assigned weight 1.0. Shallower spots are then assigned weights less than 1.0 based on the pre-computed database of dose distribution curves to achieve a spread-out Bragg peak (SOBP). The target weight is then used with the total particle count for assignment of individual particle counts for each target spot. At this step, the energy spread and beam diameter are factored in by addition of small random values to the initial energy and position of each particle. In the case of the energy spread, random numbers are chosen so that the resulting particle energies have a Gaussian distribution with the specified full width at half maximum (FWHM). Another pair of random numbers is chosen to place the particle within the specified beam diameter. Particles are distributed evenly along the beam axis. The particle list is then written on a file, which is read by the simulation program.

2.3 Target spot spacing

We incorporated a spot scanning method where the beam position and direction were fixed, while target spots along the beam direction were scanned by depth variation; i.e., active energy variation for depth modulation. All beams are assumed to be parallel to each other in this simulation (Fig. 1). This method requires a rapid alteration of the proton energy.

Our software also has the ability automatically to place target spots at locations with variable spacing based on the pre-computed database of dose profile curves in water. In the case of lateral spacing, lateral fall-off curves at the

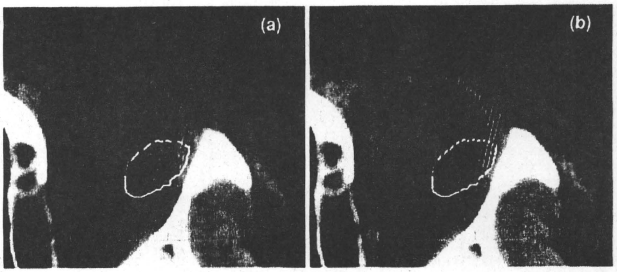

Fig. 1 Effect of beam parameters on target spot placement and beam spacing. *Blue lines* are beams. The *green polygon* is the planned target volume (PTV). *Red dots* are target spots. a 5-mm beam diameter and 10% energy spread. b 1.25-mm beam diameter and 0% energy spread, for which more target spots are generated (color figure online)

beam's pre-computed Bragg peak depth are used for determining the width (FWHM) of the beam, specifying a "spot width". The spot width is mostly affected by the beam diameter and by lateral scatter. For depth spacing, the beam's pre-computed depth–dose profile curve was used similarly for specifying a "spot depth". The spot depth is affected mostly by the energy spread.

Utilizing spot width and depth alone for spot spacing results in an uneven dose distribution within the target region due to under-dosed regions between spots. For achieving a smooth dose distribution, the spot width and the spot depth are multiplied by a "spacing factor". The spacing factor is usually less than 1.0 and has the effect of placing the spots closer together, i.e., increasing the number of spots. A spacing factor of 0.5, which we found yields a relatively smooth dose distribution while minimizing the number of target spots, was used throughout this simulation. A more detailed examination of the effect of the spacing factor on the dose distribution and the number of spots is a topic for future investigation.

2.4 Dose distribution optimization

It is difficult to predict the exact dose distribution in inhomogeneous patient volumes based on CT data alone. Therefore, after the initial Monte Carlo simulation, we fine-tuned the particle counts assigned to each target spot in the following way. The dose distribution for each target spot is calculated with the Monte Carlo simulation program and stored in separate files, one dose distribution file per target spot. The individual files are read and summed to form a complete dose distribution. The dose deposited at each target spot is compared with the dose average in the planning target volume (PTV). Spots that received less than the average dose (cold spots) are assigned more particles, and spots with a higher dose (hot spots) are assigned fewer particles. The process is repeated iteratively until it is determined that the result cannot be optimized further. Note that we do not attempt to reduce the dose deposited in critical structures; we only attempt to achieve a uniform dose distribution within the target volume in this optimization process.

2.5 Target polygon

The gross target volume (GTV) was modeled as a semi-ellipsoid with a semi-sphere base of height 4.8 mm and basal diameter 13 mm. The minimum tumor–optic disk distance was 5 mm. The tumor–macula distance was 4 mm. The values were chosen to represent a typical tumor based on data reported by Dendale et al. [16]. The GTV was generated in the planning software by specification of the tumor height, base diameter, eye center and tumor base position. A 2-mm margin was automatically added to the perimeter of the GTV to form the PTV. The volume of the PTV was .734 cm^3. The target polygon (PTV) and organs at risk (OARs) are shown in Fig. 2.

The prescribed dose was set to 54.5 Gy, which is equal to 60 cobalt Gray equivalent (CGE), assuming a relative radiobiological effectiveness (RBE) of 1.1. The tumor was assumed to be free of infiltration of the optic disk or macula. The dose distribution was normalized so that ninety-five percent of the PTV received at least 100% of the prescribed dose; i.e., "D95" for the PTV was set to 60 CGE. Four fractions in one week were assumed to be used, which is the common practice in conventional proton therapy. The effects of the energy spread and beam diameter were investigated with 60 CGE kept for D95 in each calculation.

3 Results

In the first series of simulations, the effect of the energy spread of the beam on the dose distribution was investigated. Energy spread values of 5, 10 and 15% were simulated. The beam diameter was 2.5 mm in each case. Dose distributions are shown in Fig. 3. Dose–volume

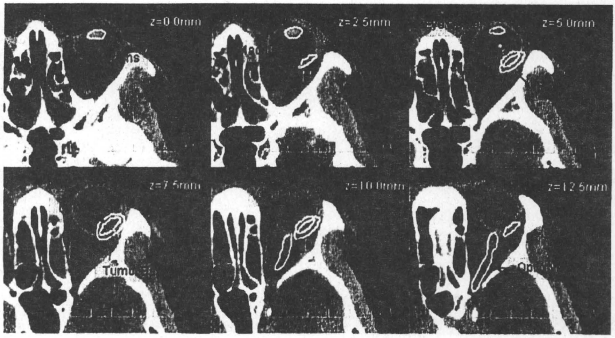

Fig. 2 Target polygons and organs at risk (OARs) used for this experiment. The inner target polygon is the *GTV*. The GTV is generated automatically by specifying the location of the tumor base and eye center. The size of the GTV is determined by specifying the basal diameter and tumor height. The outer target polygon is the *PTV* (GTV plus 2-mm margin). OARs include the lens, optic nerve macula, and optic disk (color figure online)

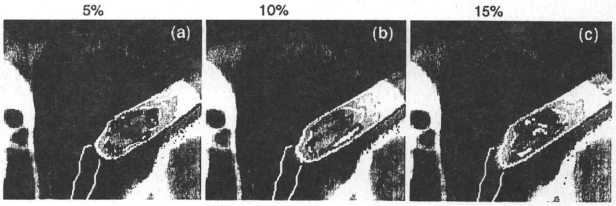

Fig. 3 Dose distributions for various values of energy spread. 5% (**a**), 10% (**b**) and 15% (**c**). Isodose lines are 125% of prescribed dose (75 CGE) *white*, 110% (66 CGE) *red*, 90% (54 CGE) *orange*, 75% (45 CGE) *yellow*, and 50% (30 CGE) *blue*. In all cases, a 2.5-mm beam width was used (color figure online)

histograms (DVHs) are shown in Fig. 4, and simulation results are summarized in Table 1. The table indicates that, at 5% energy spread, the dose to the macula and optic disc was below the tolerance values for the case that we simulated. At 10 and 15%, it was difficult to preserve critical structures located behind the distal edge of the target volume due to the elongated fall-off of the depth profile curve.

Target spot and beam characteristics are summarized in Table 2. The table shows the effect of energy spread (5, 10 and 15%) on the depth spacing and the number of target spots with a constant beam diameter (2.5 mm). The depth spacing (the distance between target spots along a beam) is increased with increasing energy spread, whereas the number of target spots is decreased with increasing energy spread.

In the second series, the effect of the beam diameter on the dose distribution was investigated. Beam diameter values of 1.25, 2.5 and 5 mm were simulated. The energy spread value for each case was 5%. Dose distributions are shown in Fig. 5, and DVHs are shown in Fig. 6. Figure 5 illustrates that the volume of hot spots in the PTV increased when the beam diameter was increased from 1.25to 2.5 mm. The simulation results are summarized in Table 3.

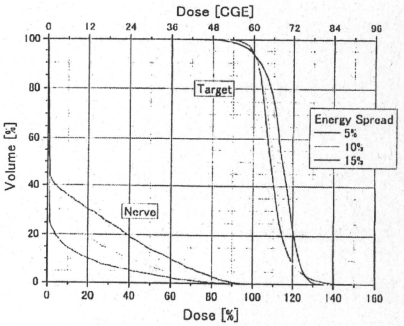

Fig. 4 DVH of PTV and optic nerve for various energy spread values. In all cases a 2.5-mm beam diameter was used (color figure online)

The table indicates that a beam diameter of less than or equal to 2.5 mm would not exceed the tolerance doses for the case that we studied. At 5-mm beam diameter, the dose to the lens becomes significant.

Table 4 indicates the effect of the beam diameter (1.25, 2.5 and 5 mm) with a fixed energy spread of 5%. The maximum and minimum values of the depth spacing were almost constant, as anticipated from the fixed energy spread. Also, the beam diameter affected the lateral spacing, as expected. The number of beams and target spots decreased significantly with an increase in the beam diameter. For a beam of 1.25 mm, nearly a thousand target spots were generated by the planning software. Such a large number of target spots would likely require a lot of time to treat.

A histogram of particle energy for a typical treatment plan is displayed in Fig. 7. In general, more particles at the higher-energy end of the spectrum are necessary because more particles are targeted at deeper locations in forming the SOBP. The energy distribution is also affected by the target shape and the incident beam direction. The energy distribution is not smooth, partly due to the discrete proton energy values used for our calculations.

Table 1 Dosimetric characteristics: energy spread

Energy spread	5%	10%	15%
Retina ≥45 CGE	1%	2%	5%
Lens ≥10 CGE	0%	0%	0%
Optic nerve ≥12 CGE	10%	20%	31%
Dose at macula (≥30 CGE)	27 (OK)	36 (NG)	42 (NG)
Dose at optic disc (≥12 CGE)	11 (OK)	18 (OK)	33 (OK)
V95[a]	98%	98%	97%

[a] Percentage volume of PTV, which received 95% of the prescribed dose (57 CGE)

Table 2 Target spot and beam characteristics: energy spread

Energy spread	5%	10%	15%
Lateral spacing (mm)	1.3	1.3	1.3
Depth spacing, minimum (mm)	0.6	1.7	3.1
Depth spacing, maximum (mm)	2.8	5.8	9.1
Number of beams	38	38	38
Number of target spots	239	102	65

Beamlet diameter was 2.5 mm for each case

4 Discussion

Many parameters and parameter combinations (such as beam diameter, energy spread, lateral spacing, depth spacing, number of beams and number of target spots) must be considered in assessing proton treatment of small superficial tumors. Realistically, some of the parameters may need to be predetermined in the clinical equipment because of mechanical or other limitations. In this study, we simulated the effect of energy spread by using a fixed beam diameter (2.5 mm), and the effect of the beam diameter by using a fixed energy spread (5%). These values were chosen because they seemed to be the most likely parameters delivered by an actual accelerator. A more thorough parameter survey is necessary for determination of the effects of every possible combination of beam parameters.

For reducing treatment times, it is desirable to reduce the number of target spots in a plan. However, there is a trade-off between the dose distribution and the number of target spots. Our results suggest that, if the beam energy and lateral spacing are predetermined, the energy spread and beam diameters must be chosen carefully with this in mind. The clinical significance of dose–volume statistics of the PTV and organs at risk must be determined for each patient.

The dose distributions shown here contain many hot spots (overdose areas). These are caused partially by the histogram normalization method, where 95% of the target volume is forced to receive at least 100% of the prescribed dose. Without normalization, cold spots were prevalent around the lateral and distal edges, especially when a large beam diameter or energy spread was used. The cold spots became prevalent when the distance from the tumor polygon edge and nearest target spot was relatively large. This resulted in DVH curves for the target volume not being as steep (selective) as they should have been. Several methods can be employed for improving the dose distributions,

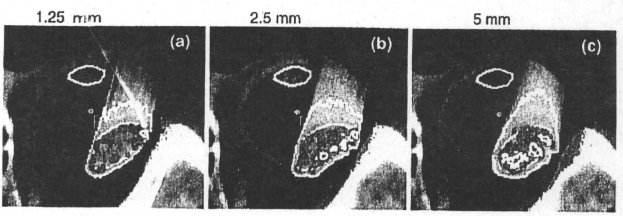

Fig. 5 Dose distribution for various values for beam diameter, 1.25 mm (**a**) 2.5 mm (**b**), and 5 mm (**c**). Isodose lines are 125% of prescribed dose (75 CGE) *white*, 110% (66 CGE) *red*, 90% (54 CGE) *orange*, 75% (45 CGE) *yellow* and 50% (30 CGE) *blue*. In all cases, we used 5% energy spread (color figure online)

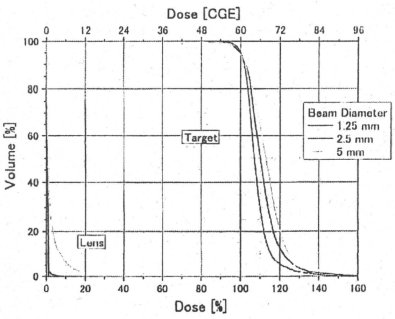

Fig. 6 DVH for PTV and optic nerve computed with various values for beam diameter. In all cases, we used 5% energy spread (color figure online)

Table 3 Dosimetric characteristics: beam diameter

Beam diameter	1.25 mm	2.5 mm	5 mm
Retina ≥45 CGE	0%	0%	1%
Lens ≥10 CGE	0%	0%	6%
Optic nerve ≥12 CGE	0%	1%	4%
Dose at macula (≥30 CGE)	13 (OK)	13 (OK)	36 (NG)
Dose at optic disc (≥12 CGE)	0.8 (OK)	3.0 (OK)	18 (NG)
V95[a]	99%	98%	98%

[a] Percentage volume of CTV, which received 95% of the prescribed dose (57 CGE)

Table 4 Spot and beam characteristics: beam diameter

Beam diameter	1.25 mm	2.5 mm	5 mm
Lateral spacing (mm)	0.7	1.4	2.6
Depth spacing, minimum (mm)	0.7	0.7	0.6
Depth spacing, maximum (mm)	2.4	2.4	2.3
Number of beams	206	57	21
Number of target spots	918	233	87

Energy spread was 5% for each case

including increasing the number of Monte Carlo events, decreasing the space between target spots and improving the optimization algorithm. Furthermore, we used a fixed spacing factor of 0.5 in this study. Introduction of a variable spacing factor for each beam may further improve the homogeneity of dose distributions. The spacing factor should be smaller near the polygon edges to prevent cold spots while maintaining a reasonable total number of spots. These are topics for future study.

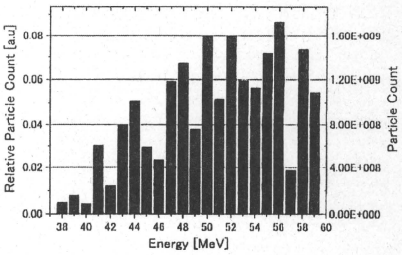

Fig. 7 A typical histogram of particle energy levels (color figure online)

In this work, doses to the macula and to the optic disc were high and above the clinical limits in some cases. This is mainly because these structures are located directly behind the distal edge of the target volume. Proton spectra that are closer to being monoenergetic may improve the final clinical outcome. The effect of energy spread for deep-seated tumors such as prostate cancer may be different from that for shallow ocular diseases and is yet to be determined.

The required proton flux can be estimated as follows. Consider a shallow tumor volume of 1 cc (1 g). If the protons deposit an average energy of 50 MeV, then each proton delivers about 8×10^{-12} J or 8×10^{-9} Gy on average. Assuming an RBE of 1.1, each proton delivers about 9×10^{-9} CGE. A typical treatment course consists of 60 CGE delivered in four fractions on consecutive days. If the irradiation time is limited to 1 min, then the accelerator must deliver 15 CGE per min or .25 CGE per s. The accelerator must therefore produce about 30 million protons per second or 4.8 pA. If such a delivery was carried out in 100 Hz repetitive pulsed laser shots, the required delivery would be in the order of 3×10^5 protons per shot.

5 Conclusion

Our simulations show that a 2.5-mm beam diameter and a 5% energy spread can be considered as a starting point for ocular cases. The dose distributions suggest that there is merit in continuing such parameter studies and considering further the potential for spot scanning proton sources.

Acknowledgments This work was supported by the Core Research for Evolutional Science and Technology (CREST), the Japan Science and Technology Agency (JST) and the Special Coordination Fund (SCF) for Promoting Science and Technology commissioned by the Ministry of Education, Culture, Sports, Science and Technology (MEXT) of Japan. K. S. is a Takuma Scholar of PMRC.

References

1. Brenner DJ, Hall EJ. Secondary neutrons in clinical proton radiotherapy: a charged issue. Radiat Oncol. 2008;86(2):165–70.
2. Kanai T, Kawachi K, Kumamoto Y, Ogawa H, Yamada Y, Matsuzawa H. Spot scanning system for proton radiotherapy. Med Phys. 1980;7(4):365–9.
3. Lomax AJ, Bohringer T, Bolsi A, Coray D, Emert F, Goitein G, et al. Treatment planning and verification of proton therapy using spot scanning: initial experiences. Med Phys. 2004;31(11):3150–7.
4. Lomax AJ, Boehringer T, Coray A, Egger E, Goitein G, Grossmann M, et al. Intensity-modulated proton therapy: a clinical example. Med Phys. 2000;28(3):317–24.
5. Tajima T. Prospect for compact medical laser accelerators. J Jpn Soc Therap Radiat Oncol. 1997;9(Suppl 2):83–5.
6. Malka V, Sven F, Lefebvre E, d'Humieres E, Ferrand R. Practicability of proton therapy using compact laser systems. Med Phys. 2004;31(6):1587–92.
7. Ma CM, Maughan RL. Point/counterpoint: within the next decade conventional cyclotrons for proton radiotherapy will become obsolete and replaced by far less expensive machines using compact laser systems for the acceleration of the protons. Med Phys. 2006;33(3):571–3.
8. Bulanov SV, Esirkepov T, Khoroshkov VS, Kuznetsov AV, Pegoraro F. Oncological hadrontherapy with laser ion accelerators. Phys Lett A. 2002;299:240–7.
9. Agostinelli S, Allisonas J, Amakoe K, Apostolakisa J, Araujo H, et al. Geant4–a simulation toolkit. Nucl Instrum Methods Phys Res A. 2003;506:250–303.
10. Carrier J, Archambault L, Beaulieu L, Roy R. Validation of Geant4, an object-oriented Monte Carlo toolkit, for simulations in medical physics. Med Phys. 2004;31(3):484–92.
11. Jiang H, Paganetti H. Adaptation of Geant4 to Monte Carlo dose calculations based on CT data. Med Phys. 2004;31(10):2811–8.
12. Sutherland K, Miyajima S, Date H. A simple parallelization of Geant4 on a PC cluster with static scheduling for dose calculations. First European workshop on Monte Carlo treatment planning, Journal of Physics: Conference Series. 2007; 74 012020.
13. Schneider W, Bortfeld T, Schlegel W. Correlation between CT numbers and tissue parameters needed for Monte Carlo simulations of clinical dose distributions. Phys Med Biol. 2000;45:459–78.
14. Iwase H, Niita K, Nakamura T. Development of a general-purpose particle and heavy ion transport Monte Carlo code. J Nucl Sci Technol. 2002;39(11):1142–51.
15. Niita K, Sato T, Iwase H, Nose H, Nakashima H, Sihver L. PHITS: a particle and heavy ion transport code system. Radiat Meas. 2006;41:1080–90.
16. Dendale R, et al. Proton beam radiotherapy for uveal melanoma: results of Curie Institute-Orsay Proton Therapy Center (ICPO). Int J Radiat Oncol Biol Phys. 2006;65(3):780–7.

総　説

日耳鼻 113：581-586，2010

「他領域からのトピックス」

頭頸部癌治療における粒子線治療の適応
—兵庫県立粒子線医療センターの経験を踏まえて—

村上　昌雄*,**

*兵庫県立粒子線医療センター
放射線科
**神戸大学大学院医学系研究科
放射線医学分野粒子線医学部門

粒子線治療はブラッグピークを持つ物理学的特性ゆえに，がん病巣への高度な線量集中が可能で，高いがん制御率と少ない副作用を両立できる．またRBE（相対的生物学的効果比）は陽子線1.1，炭素線2から3と見積もられ，X線より優れた生物学的効果を示す．陽子線または炭素イオン線を用いた粒子線治療は，わが国では2009年現在7施設において稼働し，最近急速に普及しつつある．兵庫県立粒子線医療センターは両線種が使用可能な世界唯一の施設で，2001年開院以来3,000名を超える治療実績がある．頭頸部腫瘍に対する粒子線治療は，局所進行癌でも化学療法を併用せず効果が良好で，口腔・咽頭に照射される場合でも経静脈栄養を必要とする患者はいないことから，高齢者にも優しいQOL（生活の質）の高い治療を実現できる．副鼻腔，唾液腺，口腔，咽頭，聴器から発生した悪性黒色腫，腺様嚢胞癌，腺癌など，扁平上皮癌以外の従来の放射線では抵抗性と考えられる腫瘍にも適応がある．陽子線と炭素イオン線の線量分割が異なり，厳密な比較は困難であるが，全生存率・局所制御率共に線種間の差はなかった．現在保険診療化に向けた検討が本格化している．また今後，更なる適応拡大とともに，装置の普及を目指し，機器の小型化・低価格化が課題となっている．

キーワード：粒子線治療，陽子線治療，炭素イオン線治療，頭頸部悪性腫瘍
Keywords：Particle radiotherapy, Proton therapy, Carbon-ion therapy
Head and neck malignant tumor

粒子線治療とは

電離放射線（放射線）のうち電磁波は「波」の性質を強く持つ放射線でX線やγ線を指し，重さ（質址）や電荷を持たない．一方，粒子線は「粒」の性質を強く持つ放射線で，α線，β線（電子線），陽子線，中性子線などを指し，それぞれ固有の質量を持つ．

粒子線は荷電の有無により非荷電粒子線と荷電粒子線に分類される．すなわち，負の電荷をもつ電子線，負π中間子線，正の電荷を持つ陽子線（原子番号1），ヘリウムイオン線（原子番号2），ネオンイオン線（原子番号10），炭素イオン線（原子番号12），シリコンイオン線（原子番号14），アルゴンイオン線（原子番号18），電荷を持たない中性子線に分類できる．

X線あるいは電子線は広く使われるので通常の放射線（conventional radiation）と呼ばれ，これより重い原子核あるいは原子構成粒子を加速して得られる放射線を重粒子線（heavy particle radiation）と呼ぶ．陽子（Proton）は水素（hydrogen）の原子核で，その質量は電子の1,836倍であり最も軽い原子核である．ちなみにπ中間子線の質量は電子の267倍であり，荷電重粒子線の中で最も軽い粒子線である．陽子より重たい粒子線を重イオン線（heavy-ion radiation）と呼び陽子線と区別する場合もある．負π中間子線や速中性子線は線量分布の悪さから使用されなくなり，現在，陽子線と炭素イオン線（以下，本稿ではこれらを一括して「粒子線」と呼ぶ）が世界中で最も多く使用されている．

粒子線治療は，日本および諸外国の44施設において，延べ70,000名以上の患者に対して行われている．そのうち13施設はすでに治療を終了し，現在稼働中の施設は31施設となっている[1]．日本において陽子線治療は国立

がんセンター東病院（NCCE），筑波大学陽子線医学利用研究センター，兵庫県立粒子線医療センター（HIBMC），静岡県立静岡がんセンター，若狭湾エネルギー研究センターおよび南東北がん陽子線治療センターの6施設において行われており，炭素イオン線は放射線医学総合研究所（NIRS）と兵庫県立粒子線医療センター（HIBMC）の2施設において行われている．すなわち，当センターは陽子線と炭素イオン線の両者を使用可能な施設である．今後，海外で21施設，国内では7施設の建設が計画されている．

粒子線はブラッグピーク（Bragg Peak）と呼ばれる物理学的な特徴があり，加速エネルギーに応じて体内のある一定の深さでピークを形成する．ビーム軸方向でブラッグピークを超えた領域への被爆は皆無であり，皮膚面からブラッグピークが立ち上がるまでのエントランス部分においても，腫瘍線量より低い線量に抑えることができる．これは従来のエックス線，ガンマ線，電子線にはない特徴である（図1）．この性質を利用すれば，周囲の正常組織のダメージを最小限度に抑えながら病巣に限局性に高線量を集中できる．粒子線治療は従来の放射線治療に比べると治療効果が高く副作用が少ない治療であるため，手術に取って代わる局所療法として位置づけられる[2]．

X線は単位長さあたりに与える平均エネルギーが低い放射線（低LET放射線）といわれている．陽子線治療や炭素イオン線はX線より単位長さあたりに与える平均エネルギーが高い．そのため，粒子線はX線に比べ放射線損傷が回復しにくく，組織内酸素濃度や細胞周期の影響を受けにくいという特長がある．すなわちX線を1とした場合に対する陽子線，炭素イオン線の相対的生物学的効果比（RBE：relative biological effectiveness）はそれぞれ1.1，3.0と見積もられており，いわゆる放射線抵抗性腫瘍にも効果が期待できる[3]．

これら粒子線の持つ物理学的あるいは生物学的な特徴を利用することで，人体内にある固型癌に対して周囲の正常組織への障害を極力抑えた治療ができる．

頭頸部領域における粒子線治療の特徴および適応

頭頸部領域は視覚，聴覚，味覚，嗅覚，発声，咀嚼，嚥下など，人間が日常生活を維持していくために重要な機能を有す器官が解剖学的に密集して存在し，頭側は頭蓋底を介して脳と隣接している．頭蓋底や内頸動脈などに浸潤するため，手術不適応として発見される場合も多い．また化学療法やX線治療の感受性が比較的高いリンパ腫，扁平上皮癌だけでなく，腺癌，腺様嚢胞癌，悪性黒色腫，肉腫などの放射線抵抗性腫瘍も多く発生する．

表1　兵庫県立粒子線医療センターにおける頭頸部腫瘍患者290例の背景（2001-2009. 3）

	全体（290症例）	陽子線（189例）	炭素線（101症例）
年令（歳）	19–86（中央値62）	19–86（中央値62）	19–82（中央値63）
性別（男：女）	149：141	92：97	57：44
前治療（%）			
なし	198（68）	130（69）	68（67）
化学療法	42（14）	26（14）	16（16）
手術	38（13）	27（14）	11（11）
手術＋化療	8（3）	4（2）	4（4）
放射線治療*	3（1）	1（0.5）	2（2）
化療＋放治*	1（0.3）	1（0.5）	0（0）

＊前医で途中まで照射した後，患者の希望で転医し，当センターで根治照射を施行．

タバコ，アルコールが発癌と関連することが多く，肺癌，食道癌などとの重複癌も多い．さらに社会生活を行っていく上で重要な顔貌，美容に深くかかわっているため，根治性だけでなく機能形態保存ができる治療法の開発が望まれている．粒子線治療は，従来から治療法の主体であった手術療法と放射線化学療法で解決困難であったこれらの諸問題に対して，有力な解決手段を提供できる新たな治療手段となりうる．物理的な側面からみると，頭頸部領域では陽子線2–3門のコプラナー照射でもX線の3次元原体照射以上の標的包括性向上とリスク臓器への線量軽減効果が得られており，X線に比し粒子線の持つブラッグピークの優位性が証明されている[4]．

当センターは陽子線と炭素イオン線の両者が使用できる世界唯一の施設で，2001-02年の治験を経て，現在は先進医療で治療を行っている．治療中の急性反応は軽微で，頭頸部腫瘍患者でもほぼ全例において経口摂取が可能であり，外来通院治療が全患者の約4割に達することからみても，身体に優しいがん治療が実現できているといえる．

一般には局所に限局した固型癌が粒子線治療の適応となる．化学療法の併用は行っておらず高齢者でも治療可能となる．当センターのデータでは年齢は19歳から86歳（中央値62歳）に分布していた．また新鮮例は約7割と大半を占めていたが，化学療法，手術後の再燃例も治療している（表1）．従来の放射線治療で良好な成績を示す喉頭癌は適応としていない．また，悪性リンパ腫や上咽頭扁平上皮癌のように系統的リンパ節領域照射を必要とする腫瘍も，X線治療の方が治療しやすく適応となら

表2　粒子線治療を行った頭頸部腫瘍290例・298病変の亜部位と組織型（2001-2009. 3）

	全体（298病変）	陽子線（193病変）	炭素線（105病変）
部位（%）			
上顎洞	67（22）	43（22）	24（23）
鼻腔	64（21）	40（21）	24（23）
篩骨洞	37（12）	28（15）	9（9）
口腔	33（11）	22（11）	11（10）
大唾液腺	25（8）	12（6）	13（12）
副鼻腔（その他）	22（7）	13（7）	9（9）
咽頭	20（7）	16（8）	4（4）
聴器	13（4）	12（6）	1（1）
リンパ節	7（2）	3（2）	4（4）
その他	10（3）	4（2）	6（6）
組織型（%）			
扁平上皮癌	78（26）	62（32）	16（15）
悪性黒色腫	77（26）	45（23）	32（30）
腺様嚢胞癌	63（21）	46（24）	17（16）
腺癌	21（7）	10（5）	11（10）
嗅神経芽腫	12（4）	9（5）	3（3）
未分化癌	10（3）	9（5）	1（1）
粘表皮癌	7（2）	1（0.5）	6（6）
骨肉腫	6（2）	0（0）	6（6）
肉腫（その他）	6（2）	3（2）	3（3）
その他	18（6）	8（4）	10（10）

ない．最も良い適応は副鼻腔腫瘍，唾液腺腫瘍で，その他，口腔，咽頭，聴器の腫瘍が主な対象となる．組織型は悪性黒色腫，腺様嚢胞癌，腺癌など放射線抵抗性と考えられる腫瘍の割合が多いことが，従来の放射線治療を行っている施設とは異なる特徴である．これら非扁平上皮腫瘍は粒子線治療の良い適応といえる（表2）．病期は進行したものがほとんどでT3 T4例が7割以上を占めていた（表3）．

原発巣に所属リンパ節転移を伴う場合，当センターではリンパ節郭清手術を先行していただき，原発巣のみに粒子線治療を行うことを原則としている．ただし，郭清の困難な場合や，原発巣近くの少数のリンパ節転移が原発巣と同一の照射野で治療可能な場合は，同時照射を行っている．注意すべきことはブロードビーム法を用いて広範囲の領域リンパ節に照射する場合，皮膚障害が問題となる場合がある．これは皮膚面からビーム軸方向にターゲットの最短部と最深部間の距離の最大値（厳密には密度の考慮した）がSOBP（拡大ブラッグピーク：spread out Bragg peak）の大きさを規定するため，大きな腫瘍が皮膚近くに存在する場合では，皮膚がSOBP内に入り，処方線量とほぼ等しい高線量が皮膚に照射されるためである（図1）．

表3　粒子線治療を行った頭頸部腫瘍298病変のTN因子（2001-2009. 3）

		全体	陽子線	炭素線
T病期	Tis	1	1	0
	T1	20	11	9
	T2	40	25	15
	T3	54	34	20
	T4	100	68	32
N病期	N0	191	128	63
	N1	20	15	5
	N2	23	8	15

注）TNMが定義されていない部位は除外．

粒子線治療の方法

治療の準備には固定具作成，CT，MRI撮影，治療計画装置を用いた線量計画，ボーラスコリメーター作成，リハーサル，線量測定のために1週間を要する．

治療計画は，腫瘍の発生部位（亜区域），大きさ，広がり，隣接臓器との関係，組織型，臨床病期，年齢，前治療の有無に応じて，個別に考慮する必要がある．悪性黒色腫では粘膜色素斑，腺様嚢胞癌では神経浸潤が多く，CTV（clinical target volume）を広い目に設定する場合もある．リスク臓器は脳，脊髄，眼球，視神経，聴器，耳下腺，顎関節，喉頭，皮膚などで，耐容線量内に抑える必要がある．ブロードビーム法では照射法は2-3門，ノンコプラナー照射，ボーラスコリメータを用いることが多い．

通常の放射線治療とは異なり，ビーム停止の位置・形状を任意に形成することができる．線量計算値と実測値が一致しているかどうか，患者ごとにすべての門の線量分布を事前に水ファントムを用い実測検証を行い，かつ初回照射直後には自己放射化現象を利用した線量分布の確認を行っている．粒子線治療を行うと照射部位に核の分裂が生じる．例えば陽子が照射されると体を構成する酸素原子，炭素原子はそれぞれ$^{16}O(p, pn)^{15}O$，$^{12}C(p, pn)^{11}C$の反応でポジトロン核種を生じる．炭素イオン線照射の場合は照射する炭素イオン自身がProjectile fragmentationを来し^{11}Cを生じる．^{15}Oは半減期が2分，^{11}Cは半減期が20分であるため，当センターでは初回治療直後にPET撮影を行い，治療計画画像と対比させ検証作業を行っている．

表4　頭頸部腫瘍に対する粒子線治療成績

年 報告者 機関 報告媒体	線種	例数	領域	組織型	線量 (GyE)	局所制御率 (%)	生存率 (%)	晩期有害事象
2007 Ogino[9] 国癌東 ECCO14	陽子	93	鼻副鼻腔	SCC27 ONB22 MM18 ACC13 Other13	65（58.8–70）	87（2Y）	71（2Y）	失明0，白内障3 無症候性脳壊死2 骨壊死1，髄液漏1 出血1，皮膚移植2
2007 Nishimura[10] 国癌東	陽子	14	鼻副鼻腔	ONB	65	84（5Y）	93（5Y）	Grade 3以上なし
2006 Pommier[11] MGH	陽子	23	頭蓋底	ACC	手術＋ ＋75.9CGE (70.0–76.8：X＋P)	93（5Y）	77（5Y）	G4網膜症：1 G3涙嚢鼻腔吻合：1 外反（症）再建：1 白内障手術：1
2004 Mizoe[12] 放医研	炭素	36	全領域	SCC11 AD4 MM5 ACC9 Other7	48.6–64.8	75（5Y）	33（5Y）	粘膜G2：1
	SCC扁平上皮癌，ONB嗅神経芽細胞腫，MM悪性黒色腫，ACC腺様嚢胞癌 国癌東：国立がんセンター東病院，MGH：Massachusetts General Hospital， 放医研：放射線医学総合研究所							

粒子線治療の成績

当センターで2001年8月～2009年3月に治療を開始した新鮮・根治治療症例のうち，6カ月以上経過観察可能（6カ月未満で死亡した症例を含む）であった290症例，298病変の治療成績を検討した．観察期間は3～97カ月（中央値20カ月）であった．背景因子，腫瘍の背景については表1，2，3に示した．陽子線193件（65%），炭素イオン線105件（35%）と陽子線治療の方が多い結果となっていた．これは陽子線は治験終了後2003年から治療開始できたが，炭素イオン線は2005年から一般診療可能となったことも関係する．さらに2007年4月以後は，陽子線と炭素イオン線の両者の線量分布を作成して線種を選択するようになったため，2008年では炭素イオン線（50例）の方が陽子線（33例）よりよく使用される結果となっており，最近で炭素イオン線を使用する頻度の増加が認められる．

線量分割に関しては陽子線は65GyE/26Frが最も多く125病変（65%）に用いられていたが，2007年5月から線量増加した70.2GyE/26Frが52例（27%）を占めた．炭素イオン線は57.6GyE/16Frが最も多く63例（60%），次いで線量増加した60.8GyE/16Frが29例（28%）を占めた．

全例の2年・5年局所制御率は73%・70%であり，2年・5年全生存率は70%・38%，2年・5年無再発生存率は45%・29%であった（図2）．組織型別に全生存率をみると，嗅神経芽細胞腫は5年生存率100%で最も良好で，次いで，骨肉腫以外の肉腫，腺様嚢胞癌の予後が良好であった（図3）．一方，未分化癌，腺癌，扁平上皮癌，骨肉腫などは予後が不良であった．上記のように線量分割が異なることから，厳密な比較はできないが，あえて組織型別に線種間の予後を比較したところ，扁平上皮癌，悪性黒色腫，腺様嚢胞癌，腺癌において全生存率，局所制御率共に線種間に有意差を認めなかった（図4）．今後，適切な線種選択に向けた無作為化比較試験の実施が望まれる．

他施設の治療成績を表4にまとめた．

粒子線治療の問題点と展望

1. 第一世代から第二世代粒子線治療に向かって

日本の粒子線治療施設はすべて拡大ブラッグピーク（SOBP）を形成して腫瘍全体を一度に均等に照射するブロードビーム法というビームモデュレーションで治療している（図1）．この場合，前述したように腫瘍の手前で高線領域を作り皮膚などの障害発生の原因となっている．視神経に隣接腫瘍に陽子線または炭素イオン線治療を行った後の視力障害を検討した報告では，線種間に発生頻度の差はなく1/4に失明を認めた[5]．頭蓋底腫瘍などで脳に一部照射される場合の脳障害を検討した報告では，炭素イオン線治療の方が陽子線より発生頻度が高かった[6]．これらの晩期有害事象は次世代のビームモデュレーション法であるスポットスキャンニングを用いることにより改善が期待される．さらにこの方法は腫瘍内の線量勾配を容易に制御できるので，強度変調粒子線治療（Intensity modulate particle radiotherapy）も可能となり，現行の粒子線治療よりさらに安全で腫瘍制御に優れた粒子線治療が可能となると期待される．

2. 高額医療

粒子線治療は大規模な設備が必要で，以前は物理研究所における医学利用に限られていたが，1990年米国Loma Linda大学の陽子線治療施設以来，病院設置型装置が導入されるようになり，急速に普及しつつある．わが国の粒子線治療は先進医療で行われているが，入院費・検査費などの保険診療以外に粒子線治療費として240-314万円を要する高額な医療である．民間保険業界の先進医療特約などの商品を購入した患者は安価に治療を受けられるが，多くの患者は高額の医療費の負担を強いられる．厚労省では一部の疾患で保険診療化を検討中とのことである．ただ，保険収載額が250万円を下回る低額設定となれば，多くの粒子線治療施設は経済的に維持・管理してゆくことが困難となるので，逆に普及を阻む結果となる可能性もあり慎重な配慮が必要である．

3. 陽子線と炭素イオン線の使い分け

用いた線量分割も線種ごと異なるため厳密な比較は困難であるが，各種疾患の全生存率，局所制御率に陽子線と炭素イオン線の差がないことを示した．したがって全生存率をエンドポイントとした無作為比較試験の必要性がある．すなわち両線種の全生存率に対する同等性が証明されれば，炭素イオン線より建設コストのより安価な陽子線治療の急速な世界的普及に繋がると期待される．頭頸部腫瘍は多くの組織型の腫瘍が存在するため，組織型ごとの線種間の違いを証明できれば，頭頸部領域のみならず他部位に発生した同等の組織型をもつ腫瘍の線種選択，適応判断にも示唆を与え，個別化治療へと繋がると予想される．

4. 小型加速器の開発

残念なことに粒子線治療はいまだ実験的，特殊な施設でのみ行われている研究段階の医療と多くの医療者から認識されている．普及を阻む最大の要因は建設コストが高額（70-130億円）となるためである．従来型の加速器であるシンクロトロンやサイクロトロンを用いないレーザー駆動型加速器は1979年田島ら[7]により提唱された．装置が小型であるため建設コストが従来型の1/10位になるほか，極短パルスによる効果，レーザー強度可変による陽子線エネルギー調整，微細なスポットスキャンニングなど従来型加速器にはない特徴があり，世界中で研究が進みつつある．われわれも原子力機構と協働し，レーザー駆動小型粒子線治療の開発に着手している[8]．

参考文献

1) Particle Therapy Co-Operative Group: Particle therapy facilities in operation. 2009. Accessed at http://ptcog.web.psi.ch/ on 26 October 2009.
2) 阿部光幸，菱川良夫，村上昌雄：陽子線と炭素線治療—癌患者の速やかな社会復帰を目指す．実験医学 2004; 22: 2111-2116.
3) Kagawa K, Murakami M, Hishikawa Y, et al: Preclinical biological assessment of proton and carbon ion beams at hyogo ion beam medical center. Int J Radiation Oncology Biol Phys 2002; 54: 928-938.
4) Cozzi L, Fogliata A, Lomax A, et al: A treatment planning comparison of 3D conformal therapy, intensity modulated photon therapy and proton therapy for treatment of advanced head and neck tumours. Radiother Oncol 2001; 61: 287-297.
5) Demizu Y, Murakami M, Miyawaki D, et al: Analysis of vision loss caused by radiation-induced optic neuropathyafter particle therapy for head-and-neck and skull-base tumors adjacent to optic nerves. Int J Radiat Oncol Biol Phys; In press.
6) Miyawaki D, Murakami M, Demizu Y, et al: Brain Injury After Proton Therapy or Carbon Ion Therapy for Head and Neck Cancers and Skull Base Tumors. Int J Radiat Oncol Biol Phys; In press.
7) Tajima T, Dawson M: Laser electron accelerator. Phys Rev Lett 1979; 43: 267.
8) Murakami M, Hishikawa Y, Miyajima S, et al: Radiotherapy using a laser proton accelerator, Laser-Driven Relativistic Plasmas Applied for Science, Industry, and Medicine. 2008: pp 275-300.
9) Ogino T, Kawashima M, Zenda S, et al: Proton beam

therapy for nasal cavity and paranasal sinus malignancies. 2007; ECCO14.
10) Nishimura H, Ogino T, Kawashima M, et al: Proton-beam therapy for olfactory neuroblastoma. Int J Radiat Oncol Biol Phys 2007; 68: 758-762.
11) Pommier P, Liebsch NJ, Deschler DG, et al: Proton beam radiation therapy for skull base adenoid cystic carcinoma. Arch Otolaryngol Head Neck Surg 2006; 132: 1242-1249.
12) Mizoe J, Tsujii H, Kamada T, et al: Dose escalation study of carbon ion radiotherapy for locally advanced head-and-neck cancer. Int J Radiat Oncol Biol Phys 2004; 60: 358-364.

連絡先 〒679-5165 兵庫県たつの市新宮町光都1-2-1
兵庫県立粒子線医療センター放射線科
村上昌雄

Int. J. Radiation Oncology Biol. Phys., Vol. 76, No. 1, pp. 277–286, 2010
Copyright © 2010 Elsevier Inc.
Printed in the USA. All rights reserved
0360-3016/10/$–see front matter

ELSEVIER

doi:10.1016/j.ijrobp.2009.05.065

PHYSICS CONTRIBUTION

THE DEVELOPMENT AND CLINICAL USE OF A BEAM ON-LINE PET SYSTEM MOUNTED ON A ROTATING GANTRY PORT IN PROTON THERAPY

TEIJI NISHIO, PH.D.,*† AYA MIYATAKE, M.SC.,‡ TAKASHI OGINO, M.D.,* KEIICHI NAKAGAWA, M.D.,† NAGAHIRO SAIJO, M.D.,§ AND HIROYASU ESUMI, M.D.‖

From the *Particle Therapy Division, Research Center for Innovative Oncology, National Cancer Center, Kashiwa; †Department of Radiology, Graduate School of Medicine, University of Tokyo; ‡Department of Nuclear Engineering and Management, Graduate School of Engineering, University of Tokyo; §Deputy Director, National Cancer Center, Kashiwa; and ‖Director, National Cancer Center, Kashiwa

Purpose: To verify the usefulness of our developed beam ON-LINE positron emission tomography (PET) system mounted on a rotating gantry port (BOLPs-RGp) for dose–volume delivery-guided proton therapy (DGPT).
Methods and Materials: In the proton treatment room at our facility, a BOLPs-RGp was constructed so that a planar PET apparatus could be mounted with its field of view covering the iso-center of the beam irradiation system. Activity measurements were performed in 48 patients with tumors of the head and neck, liver, lungs, prostate, and brain. The position and intensity of the activity were measured using the BOLPs-RGp during the 200 s immediately after the proton irradiation.
Results: The daily measured activity images acquired by the BOLPs-RGp showed the proton irradiation volume in each patient. Changes in the proton-irradiated volume were indicated by differences between a reference activity image (taken at the first treatment) and the daily activity-images. In the case of head-and-neck treatment, the activity distribution changed in the areas where partial tumor reduction was observed. In the case of liver treatment, it was observed that the washout effect in necrotic tumor cells was slower than in non-necrotic tumor cells.
Conclusions: The BOLPs-RGp was developed for the DGPT. The accuracy of proton treatment was evaluated by measuring changes of daily measured activity. Information about the positron-emitting nuclei generated during proton irradiation can be used as a basis for ensuring the high accuracy of irradiation in proton treatment. © **2010 Elsevier Inc.**

Dose–volume delivery guided proton therapy (DGPT), Beam ON-LINE PET system on rotating gantry port (BOLPs-RGp), Target nuclear fragment reaction.

INTRODUCTION

Proton therapy is a form of radiotherapy that enables the concentration of a dose onto a tumor by the use of a scanned or modulated Bragg peak. Therefore, it is very important to evaluate the proton-irradiated volume accurately.

Recently, to ensure the high accuracy of proton therapy, imaging studies of positron-emitting nuclei that are generated by target nuclear fragment reactions involving incident protons and nuclei from a patient's body have been performed (1–14). The annihilation gamma rays from the positron-emitting nuclei were measured by a positron emission tomography (PET) system (specifically a beam OFF-LINE PET system using commercial PET apparatus or PET-computed tomography [CT] apparatus postirradiation or a beam ON-LINE PET system in a proton treatment room). The beam OFF-LINE PET system using the commercial PET-CT apparatus has the advantage of being able to easily acquire fusion images and the ability to reconstruct three-dimensional images. However, the time required for the movement of the patient to the PET room (10–30 min) and the resulting deterioration of the statistical accuracy of the acquired data are large disadvantages. With the beam ON-LINE PET system, capturing a large view and the acquisition of three-dimensional images are difficult because of geometrical problems caused by the beam direction and the PET apparatus (7, 15, 16).

Reprint requests to: Teiji Nishio, Ph.D., Particle Therapy Division, Research Center for Innovative Oncology, National Cancer Center, Kashiwa 6-5-1 Kashiwano-ha, Kashiwa-shi, Chiba 277-8577, Japan. Tel: (+81) 4-7133-1111; Fax: (+81) 4-7134-7048; E-mail: tnishio@east.ncc.go.jp

Conflict of interest: none.

Supported by Health and Labour Science Research Grants from the Japanese Government.

Acknowledgment—The authors would like to thank the staff members of the Proton Radiotherapy Department of the National Cancer Center, Kashiwa for their help and the members of SHI Accelerator Service, Ltd., and Accelerator Engineering, Inc., for operating of the proton apparatus. We also acknowledge T. Okamoto of Hamamatsu Photonics, K. K., T. Tachikawa of Sumitomo Heavy Industries, Ltd., and H. Oka of SGI Japan, Ltd., for their technical support.

Received Jan 6, 2009, and in revised form May 28, 2009. Accepted for publication May 29, 2009.

The ability to take daily PET images with a high statistical accuracy while the patient remains in the proton irradiation room is a large advantage. Besides, availability of a cone beam (CB) CT system or CT apparatus in the irradiation room can offer the possibility of daily and in situ monitoring of the patient's anatomy. A prototype beam ON-LINE PET system (BOLPs) was previously constructed for basic research (10), and verification of the proton-irradiated volume in a patient's body was confirmed using a PET apparatus and a PET-CT apparatus (beam OFF-LINE PET system) (13).

A BOLPs mounted on a rotating gantry port (BOLPs-RGp) was constructed in our proton treatment room. Activity measurement and PET imaging were performed in 48 patients with tumors of the head and neck, liver, lungs, prostate, and brain during proton treatment at our facility. The position and intensity of the activity were measured daily using the BOLPs-RGp immediately after proton irradiation. Using the activity measurement, we were able to confirm whether the proton beam irradiation of the tumor was reproducibly performed during the treatment period. Moreover, changes in the activity distribution were observed as the volume of the tumor changed, and these changes were related to the delivery dose, changes in the body shape and position of the patient, and the physiologic changes. The PET images from the BOLPs-RGp were sufficient to provide high-quality proton treatment.

METHODS AND MATERIALS

Design of a beam ON-LINE PET system mounted on an RGp

Via the detection of pairs of annihilation gamma rays emitted from the generated radioactive nuclei of a patient's body, the BOLPs-RGp is designed to determine the position and activity of the positron-emitting nuclei generated in patients by proton irradiation. Figure 1 is a picture of the BOLPs-RGp. The BOLPs-RGp was developed as a standardized system for use with proton therapy devices. During proton therapy, the detector heads have many degrees of freedom and the system allows remote control adaptation to each new proton beam condition and a patient's position. As a result, the measurement of the activity distribution is simple.

A planar positron imaging system (Hamamatsu Photonics K. K., Hamamatsu, Japan) (17) was newly arranged for the BOLPs-RGp. In comparison to the system used previously (10), the 24 detector units mounted on each detector head were increased to 36 detector units, and each unit was composed of 11 × 10 arrays of BGO ($Bi_4Ge_3O_{12}$) crystals with a crystal size of 2 × 2 × 20 mm^3. Furthermore, the 2,400 crystals were increased to 3,600 crystals. The gap of each unit became 3.3 mm from 11.0 mm for minimizing dead space in the detector. The field of view (FOV) became 164.8 × 167.0 mm^2 from 120.8 × 186.8 mm^2. The maximum field size is 185.0 × 185.0 mm^2 in the rotating gantry port with the BOLPs-RGp. Therefore, the FOV can almost cover each treatment site of the head and neck, liver, lungs, prostate, and brain for a proton treatment in our facility. However, in case of prostate, the depth activity distribution is not measured in the entrance of the incident proton beam. The BOLPs-RGp was mounted on and the center of its detection area was aligned with the iso-center of the rotating gantry in the treatment room of the proton therapy facility at our center. A PET image reconstructed by a back-projection method

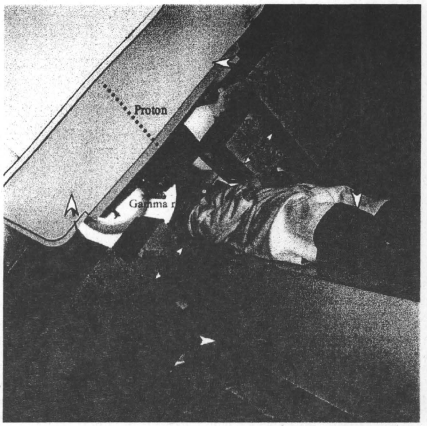

Fig. 1. Setup of the BOLPs-RGp, which is mounted on the rotating gantry port of our proton treatment room.

along the axis of the proton beam direction is always included in the FOV of the opposing detectors together with the axis of the rotating angle of the gantry system. The distance between the two opposing detector heads of the BOLPs-RGp can be adjusted from 30 to 100 cm. When the activity is not being measured, the detector head is stored inside the wall of the gantry device. The position resolution of this system is about 2 mm for the full width at half maximum in the case of use of ^{22}Na point source. The maximum data collection rate for the coincident detection of pair annihilation gamma rays is about 4,000 counts/s/cm^2 (kcps/cm^2). The accuracy of the measurements of activity distribution by this system was verified by a prototype beam ON-LINE PET system (10). The measured data are stored using in the software's list mode format. The activity image is renewed every second. The information of the on-off time points of beam irradiation is recorded in the data, and the image can be restructured according to this information. The PET data from the irradiation field of each patient are managed throughout each treatment day.

The detection efficiency of the distance between the detector heads was calibrated by using the thin-flat acrylic container filled with ^{18}F-solution. The calibration is used for a correction of the imaging uniformity and the detection sensitivity. The attenuation coefficient of 511-keV gamma rays in the patient's body was calculated by the patient's CT image data. They are used for a construction of the activity imaging. The correction of the photon scattering in the patient's body is not considered for the activity imaging. Furthermore, the photons scattered in the patient's body outside the FOV are detected by the effect of the geometry of the detector head. Therefore, the activity image is contaminated by about 10% background in this system. As the result, the position resolution of the activity distribution will become large more than 2 mm in the clinical case of a proton therapy.

Activity measurement in a patient during proton treatment

The measurement of activity was performed daily in 48 cases involving tumors of the head and neck, liver, lungs, prostate, and brain